MIT Libraries | DSpace@MIT

MIT Open Access Articles

Versatile RNA Interference Nanoplatform for Systemic Delivery of RNAs

The MIT Faculty has made this article openly available. ***Please share*** how this access benefits you. Your story matters.

Citation: Choi, Ki Young, Oscar F. Silvestre, Xinglu Huang, Kyung Hyun Min, Gregory P. Howard, Naoki Hida, Albert J. Jin, et al. "Versatile RNA Interference Nanoplatform for Systemic Delivery of RNAs." ACS Nano 8, no. 5 (May 27, 2014): 4559–4570. © 2014 American Chemical Society

As Published: http://dx.doi.org/10.1021/nn500085k

Publisher: American Chemical Society (ACS)

Persistent URL: http://hdl.handle.net/1721.1/97479

Version: Final published version: final published article, as it appeared in a journal, conference proceedings, or other formally published context

Terms of Use: Article is made available in accordance with the publisher's policy and may be subject to US copyright law. Please refer to the publisher's site for terms of use.

Massachusetts Institute of Technology

Versatile RNA Interference Nanoplatform for Systemic Delivery of RNAs

Ki Young Choi,[†,‡,∥] Oscar F. Silvestre,[†,∥] Xinglu Huang,[†] Kyung Hyun Min,[†] Gregory P. Howard,[†] Naoki Hida,[†] Albert J. Jin,[‡] Nicole Carvajal,[§] Sang Wook Lee,[⊥] Jong-In Hong,[⊥] and Xiaoyuan Chen[†,*]

[†]Laboratory of Molecular Imaging and Nanomedicine, National Institute of Biomedical Imaging and Bioengineering, National Institutes of Health, Bethesda, Maryland 20892, United States, [‡]Department of Chemical Engineering and the David H. Koch Institute for Integrative Cancer Research, Massachusetts Institute of Technology, Cambridge, Massachusetts 02139, United States, [§]Laboratory of Cellular Imaging and Macromolecular Biophysics, National Institute of Biomedical Imaging and Bioengineering, National Institutes of Health, Bethesda, Maryland 20892, United States, and [⊥]Department of Chemistry, Seoul National University, Seoul, Korea. [∥]These authors contributed equally to this project.

ABSTRACT Development of nontoxic, tumor-targetable, and potent *in vivo* RNA delivery systems remains an arduous challenge for clinical application of RNAi therapeutics. Herein, we report a versatile RNAi nanoplatform based on tumor-targeted and pH-responsive nanoformulas (NFs). The NF was engineered by combination of an artificial RNA receptor, Zn(II)-DPA, with a tumor-targetable and drug-loadable hyaluronic acid nanoparticle, which was further modified with a calcium phosphate (CaP) coating by *in situ* mineralization. The NF can encapsulate small-molecule drugs within its hydrophobic inner core and strongly secure various RNA molecules (siRNAs, miRNAs, and oligonucleotides) by utilizing Zn(II)-DPA and a robust CaP coating. We substantiated the versatility of the RNAi nanoplatform by demonstrating effective delivery of siRNA and miRNA for gene silencing or miRNA replacement into different human types of cancer cells *in vitro* and into tumor-bearing mice *in vivo* by intravenous administration. The therapeutic potential of NFs coloaded with an anticancer drug doxorubicin (Dox) and multidrug resistance 1 gene target siRNA (siMDR) was also demonstrated in this study. NFs loaded with Dox and siMDR could successfully sensitize drug-resistant OVCAR8/ADR cells to Dox and suppress OVCAR8/ADR tumor cell proliferation *in vitro* and tumor growth *in vivo*. This gene/drug delivery system appears to be a highly effective nonviral method to deliver chemo- and RNAi therapeutics into host cells.

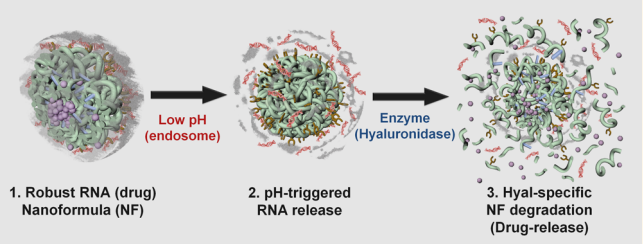

KEYWORDS: RNAi · nanomedicine · gene and drug delivery · hyaluronic acid · cancer therapy

The RNA interference (RNAi) technique based on small interfering RNA (siRNA) or microRNA (miRNA) has shown great potential for cancer therapy given its unique sequence-specific gene silencing effect.[1−3] However, clinical translation of RNAi has stalled over a decade due to the difficulties in delivering RNAs into the tumor tissues and, more importantly, into the tumor cells *in vivo*. The key to overcoming this challenge is to deliver RNAs effectively into host cells. A number of RNA delivery systems based on cationic polymers, lipids, or amino acids have been developed for *in vitro* applications,[4−6] topical delivery *in vivo*,[7,8] or a limited number of systemic delivery systems *in vivo* that are mainly confined to liver or lung targeted applications.[9,10] The development of simple, safe, and versatile platforms for systemic delivery of RNAis to tumor cells remains a grand challenge.[11−13] To overcome these limitations, herein, we report a versatile RNAi nanoplatform based on tumor-targeted and pH-responsive RNA nanoformulas (NFs) that can deliver a wide range of RNAi agents into tumor cells *in vivo* by systemic administration. We substantiated the versatility of this RNAi delivery system by demonstrating its effective delivery of both siRNA and miRNA into three different human cancer cell lines (144B, DU145, and HCT116) and into HCT116 tumor-bearing mice by intravenous injection. Systemic administration of this nanocarrier system demonstrates its ability to overcome obstacles met under physiological conditions.

* Address correspondence to shawn.chen@nih.gov.

Received for review January 6, 2014 and accepted April 29, 2014.

Published online April 29, 2014
10.1021/nn500085k

© 2014 American Chemical Society

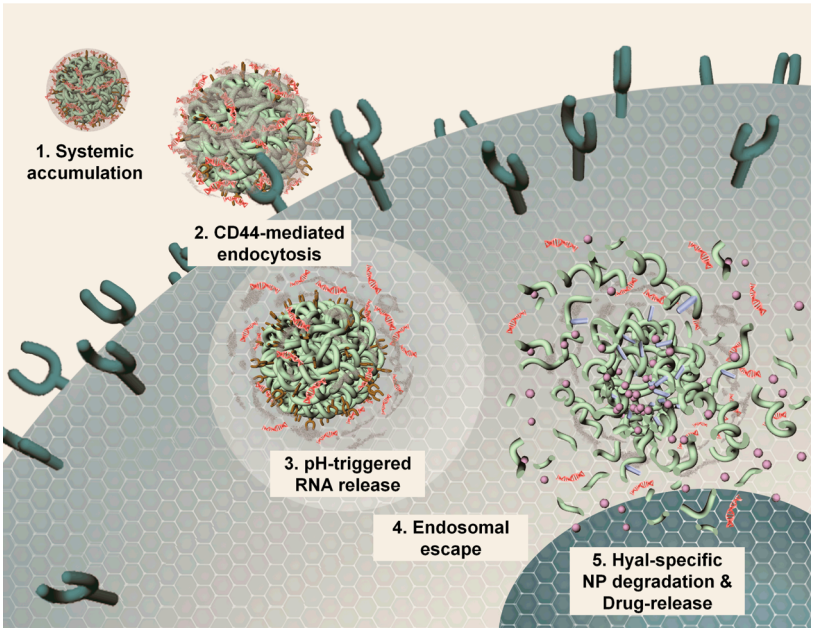

Figure 1. Schematic illustration of hypothetical tumor-targeting, cellular uptake, RNA release, and degradation pathway of CaP-HDz/RNA-NF. (1,2) The nanoformula (NF) can deliver both RNAs and lipophilic drug molecules into the tumor cells *via* systemic accumulation as well as CD44-mediated endocytosis. (3) NF releases RNAs in late endosomes or early lysosomes (pH ~4.5−5.5) with the CaP layer dissolved in the acidic environment, releasing calcium and phosphate ions. (4) NFs and RNA molecules can escape from endosomes likely due to the increased osmotic pressure in endosomes, which can cause endosomal swelling and consequent endosomal escape of RNAs. After the endosomal escape, RNAs can be distributed evenly into the cytosol of cancer cells, which results in selective suppression of target genes. (5) NFs can be further degraded by HA enzyme, hyaluronidases (Hyals), resulting in collapse of nanostructure and release of all the payloads (*e.g.*, lipophilic small-molecule drugs).

Several critical factors should be considered when designing potent *in vivo* RNA delivery systems: (i) securing of RNAs to delivery carriers; (ii) *in vivo* tumor targeting and cell permeation; (iii) RNA release from delivery carriers; (iv) homogeneous distribution of RNAs in the cytosol after endosomal escape.[3,12,13] To meet these requirements, we engineered a nanocarrier (NC) that can strongly secure RNA molecules using artificial RNA receptors, deliver RNAs into the tumor cells *via* receptor-mediated endocytosis, and release RNAs into the cytosol of cancer cells (Figure 1).

The NC system is mainly based on tumor-cell-specific and drug-loadable HA-based nanoparticles (HA-NPs) that we recently developed.[14,15] The HA-NPs are formed by self-assembly of engineered hyaluronan-5β-cholanic acid (HA-CA) conjugates, as a NC platform for hydrophobic, small-molecule anticancer drugs.[16,17] The main components are made of naturally occurring glycosaminoglycan HA conjugated with a bile acid analogue, CA (Supporting Information Figure S1c). The use of naturally occurring biomolecules decreases the likelihood of safety concerns that are associated with synthetic materials. These are ideal NCs for cytotoxic/anticancer drugs because HA-NPs can selectively target tumors not only by passive accumulation in the leaky vasculature of tumor tissues but also by active binding onto and penetration into cancer cells *via* receptor-mediated endocytosis after binding to HA receptor, CD44, which is overexpressed on various tumors.[18−20]

Although the HA-NP serves as an ideal nanocarrier platform for delivery of small-molecule anticancer drugs, it is, however, not by itself capable of RNA delivery. The HA-NP is composed of a highly anionic polymer that cannot form polyelectrolyte complexes with anionic RNA for facile cellular delivery. In this study, therefore, an artificial RNA receptor, Zn(II)-dipicolylamine (DPA/Zn) which has a high affinity for RNAs *via* specific interactions between coordinated zinc ions of DPA and anionic phosphates of the RNA,[21−23] was utilized to functionalize the HA-NP system (Supporting Information Figure S1d). Unlike most reported gene delivery systems that are based on cationic derivatives or chemically modified RNAs, this nanoformula exploits an engineered RNA receptor, DPA/Zn. This DPA/Zn-labeled HA-NP (HDz) NC system takes advantage of the phosphate binding properties of DPA/Zn to bind RNAs and tumor cell targetability of HA-NP. Moreover, since RNA agents and hydrophobic anticancer drugs can be simultaneously loaded onto the surface and inner cores of this HDz nanocarrier, respectively, in a facile manner, this nanocarrier can exert synergistic effects associated with codelivery of these two different therapeutic avenues. This combination enables intracellular delivery of RNAs and/or chemotherapeutics *in vivo* with enhanced cell permeability, tumor targetability, and low toxicity.

Despite the strong complexation of RNAs with HDz-NCs, HDz/RNA-NFs still face difficulties in practical use because the phosphate-specific binding between RNAs and DPA/Zn can be perturbed by endogenous phosphate anions in the physiological environment.[24] Given considerably high phosphate concentration in the cell culture medium or the bloodstream, the NFs necessitate further protection from phosphate molecules *in vitro* and *in vivo*. Therefore, we added complementary calcium phosphate (CaP) layers onto the HDz/RNA-NFs by *in situ* mineralization of sequentially added calcium and phosphate ions. The robust CaP precipitate coating significantly increases the NFs' ability to secure RNAs under phosphate-rich physiological conditions.

Moreover, the CaP coating facilitates pH-dependent RNA release and endosomal escape. The CaP precipitate rapidly dissolves at acidic pH (pH <6), releasing nontoxic calcium and phosphate ions.[25] After CD44-mediated endocytosis, the CaP layer can be dissolved in late endosomes or early lysosomes (pH 4.5−5.5), releasing calcium and phosphate ions. As the CaP layer is removed, RNAs incorporated onto the HDz-NCs can be uncovered. The phosphate ions released from the nanoformulas competitively bind with DPA/Zn receptors and, consequently, can trigger RNA release from the HDz/RNA-NFs. The HA-based backbone can be degraded by HA enzymes, hyaluronidases (Hyals), inside the tumor cells,[28,29] which result in NP collapse and subsequent release of small-molecule chemotherapeutics or other payloads from the NFs. Furthermore, like polymers with low pK_a amine groups, the ionic components released from CaP-HDz/RNA-NFs can deplete protons in an acidic environment, and they are capable of buffering the endosomes, increasing osmotic pressure of endosomes, leading to endosomal swelling and lysis, which subsequently results in release of nucleic acids into the cytoplasm as previously reported.[26,27]

RESULTS AND DISCUSSION

The engineered nanocarrier for RNA delivery is composed of four major components (Figure 2a): (i) a hydrophilic hyaluronan (HA) shell as CD44-targeting ligand; (ii) hydrophobic 5β-cholanic acid (CA) inner core as a drug reservoir; (iii) a phosphate receptor Zn(II)-dipicolylamine (DPA/Zn), as a RNA binding site; (iv) a calcium phosphate layer. To prepare the NC, we functionalized the HA-NPs with phosphate receptor, DPA/Zn, to serve as a RNA binding site (Supporting Information Figure S1d). First, hydrophilic HA and hydrophobic CA molecules were conjugated as previously reported;[14,15] the amphiphilic conjugate can form self-assembled nanoparticles (HA-NPs) that deliver hydrophobic, small-molecule anticancer drugs.[16,17] Second, to prepare the HDz nanocarrier, amine-functionalized bis(DPA) molecules were covalently conjugated with the carboxylic groups on the HA backbone of HA-NPs.[24] The ^{1}H NMR analysis indicated that 15.5 ± 3.4 molecules of CA and 28.5 ± 4.2 molecules of bis(DPA) were bound onto the HA backbone of HDz conjugate (Supporting Information Figure S2). The HDz conjugates were self-assembled in aqueous solution, forming nanosized particles with an average hydrodynamic diameter of 94.3 ± 3.5 nm (Figure 2b).

The HDz-NCs were readily complexed with a variety of RNAi agents (siRNA, miRNA, or oligonucleotide) by mixing RNAs with NCs. The gel electrophoresis images showed significant retardation of RNA molecules (1 μL, 266 ng, 20 pmol) formulated with HDz-NCs (2 μL, 2 μg, 7.3 pmol), indicating successful incorporation of RNAs onto the HDz-NCs (Figure 2c,e,f). After HDz-NCs were formulated with RNA molecules, the mean diameter of HDz/RNA-NFs increased by approximately 15 nm (from 94.3 ± 3.5 to 108.8 ± 1.8 nm), and the surface charge decreased from −25.1 ± 0.9 to −30.9 ± 2.0 mV due to the incorporation of negatively charged RNA molecules onto the HDz-NC (Figure 2b). The incorporation of RNAs onto HDz-NCs is based on the strong, selective binding of DPA/Zn toward diphosphate groups of the RNA backbone. The binding of RNAs with DPA/Zn ligands was disrupted by the addition of excess phosphate ions (Na_3PO_4, 1.2 μmol) (Figure 2d) but was not affected by other molecules (*i.e.*, NaCl, $MgCl_2$).[24]

In an effort to better secure RNAs as well as to facilitate pH-dependent RNA release, we modified the HDz/RNA-NCs with a calcium phosphate layer by *in situ* mineralization onto the NFs. RNAs incorporated onto the NFs are stable even after incubation with an excess amount of phosphate ions (Na_3PO_4, 1.2 μmol), indicating that the CaP layer can help protect RNAs under physiological conditions (pH ~7.4) (Figure 2d). The CaP-HDz/RNA-NFs exhibited slightly negative surface charge (−5 ± 1.1 mV) and 196 ± 35.6 nm hydrodynamic size (Figure 2b). AFM analyses demonstrated that over 95% of the CaP-HDz/RNA-NFs were uniformly dispersed as single, spherical particles (124.2 ± 47.8 nm). Clusters with relatively large particle sizes (310.0 ± 31.3 nm) were found in less than 5% of the whole population in AFM images (Figure 2e,f). The cluster formation was not detected in the DLS measurement. The smaller size distribution of NFs and the cluster formation found in the AFM analyses may be attributed to the drying process of the AFM sample preparation.

With phosphate ions released from the NFs in acidic environment, RNA release can be triggered by competitive binding between the CaP layer released phosphate anions and RNA complexes for DPA/Zn receptors. In this study, the pH-dependent RNA release profiles of CaP-HDz/RNA-NFs were studied using gel electrophoresis. At neutral pH (pH 7.4), RNAs were firmly incorporated with CaP-HDz-NCs, showing

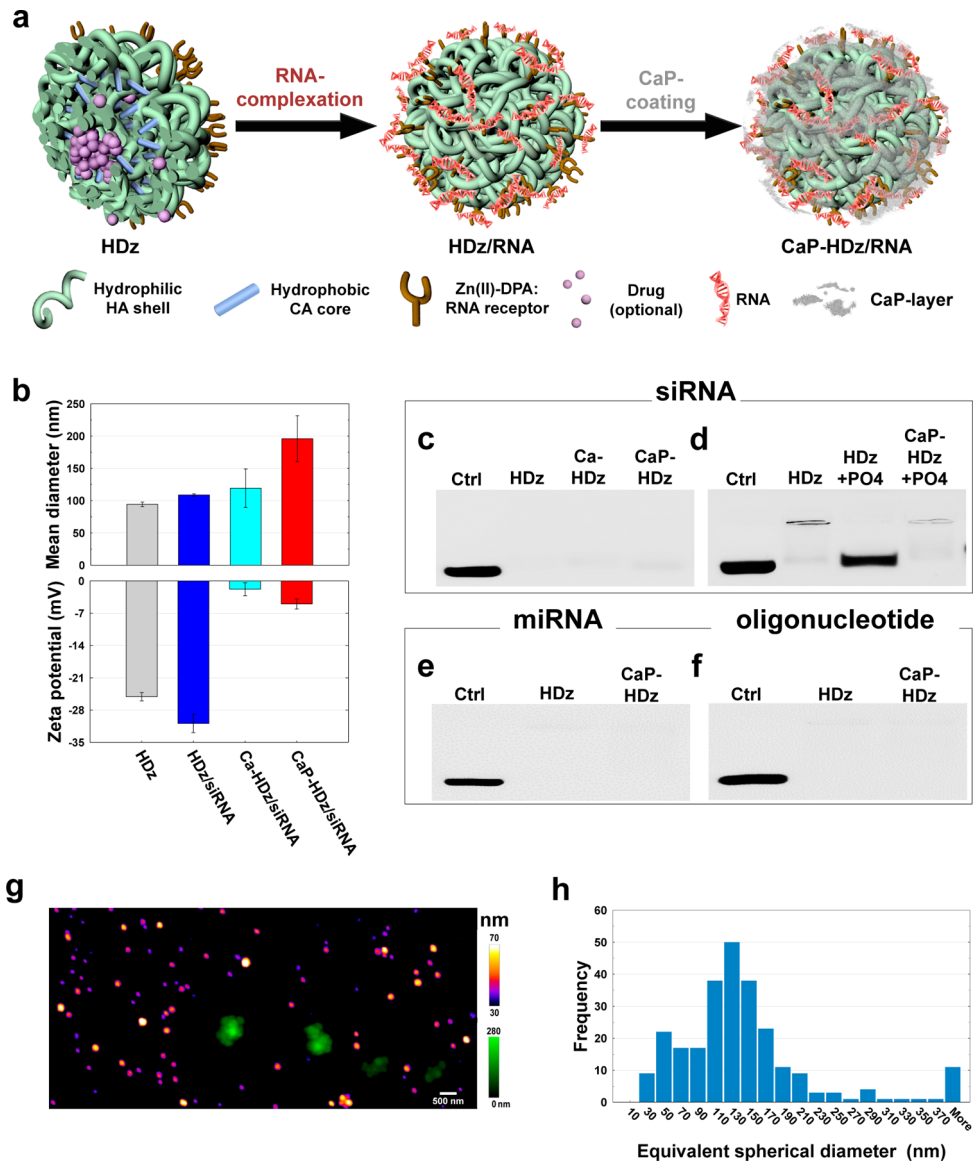

Figure 2. Preparation of CaP-HDz/RNA-NF. (a) NFs can strongly secure RNA molecules (and small-molecule lipophilic drugs if needed) using artificial RNA receptors (Zn/DPA) as well as a CaP-layer. (b) Zeta-potential results of HDz-NP, HDz/siRNA-NF, Ca-HDz/siRNA-NF, and CaP-HDz/siRNA NF. Electrophoretic retardation analysis of siRNA (c,d), miRNA (e), and oligonucleotide (f) (all at 10 pmol) binding with HDz and CaP-HDz-NP (all at 2 μg of HDz-NP). The siRNA, miRNA, and oligonucleotide are securely complexed with HDz and CaP-HDz at neutral pH (pH 7.4). Release of siRNA from HDz/siRNA was observed after addition of phosphate ions. However, siRNA molecules were secured on CaP-HDz/siRNA-NFs with phosphate ions added. AFM image of representative CaP-HDz/siRNA-NFs (g) and histogram of the diameter (h). Scale bar, 500 nm.

substantial retardation of RNA release; however, significant RNA release (52.8 ± 1.3%) was observed at slightly acidic pH (5.0 or 6.0 pH), implying that the NFs can release RNAs in acidic intracellular compartments such as endosomes (pH ~5.0) and lysosomes (pH ~4.5) (Figure 3b,c). Meanwhile, the NP degradation and drug release behavior of NFs were monitored using fluorescence microscopy. As a fluorescent model drug, Oregon green labeled paclitaxel (PTX-OG) was loaded into the CaP-HDz/siRNA-NFs. After loading, the fluorescence of PTX-OG was highly quenched, indicating compact encapsulation of PTX-OG molecules in the hydrophobic cores of NFs. However, when the NFs were exposed to Hyal, fluorescence intensities were significantly recovered due to the release of PTX-OG from the NFs. With the increase of Hyal concentration, the NF backbone was further degraded and additional PTX-OG molecules were released, thus increasing the fluorescence intensity (Figure 3d,e).

In addition, we tested the stability of siRNA complexed with CaP-HDz-NCs in the physiological condition (Supporting Information Figure S4). siRNA formulated with CaP-HDz-NCs and free siRNA (15 pmol) were incubated in the mouse serum for 1, 6, and 24 h at 37 °C. Sequentially, the samples were incubated at pH 5 for 20 min to emulate the endosome/lysosome acidic environment. After the incubation, intact RNA amount in the samples was evaluated by gel electrophoresis

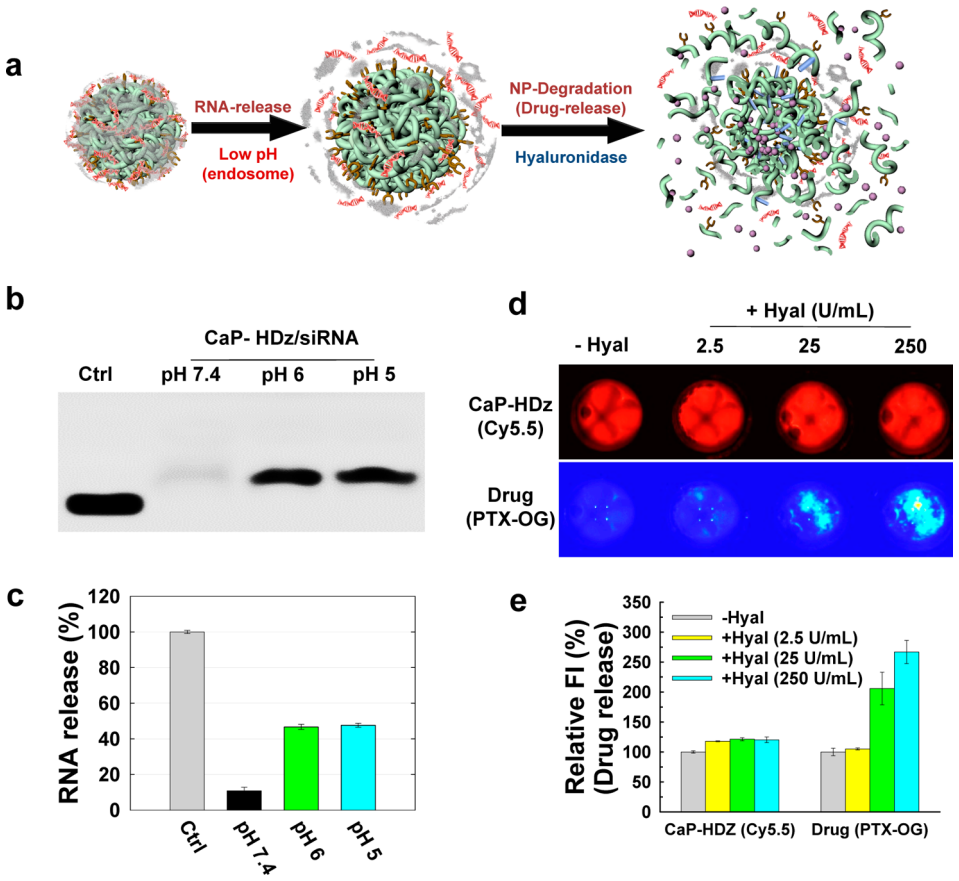

Figure 3. (a) RNA release and degradation mechanism of CaP-HDz/siRNA-NF. With the CaP layer dissolved in late endosomes or early lysosomes (pH 4.5−5.5), the NFs can free RNA molecules. Phosphate ions released from the NFs competitively bind with DPA/Zn receptors and, consequently, can trigger RNA release from the HDz/RNA-NFs. Furthermore, the HA-based backbone can be degraded by Hyals in the tumor cells, which can result in NF collapse and release of drug payloads from the NFs. (b,c) siRNA complexed with CaP-HDz-NFs can be firmly secured at neutral pH (pH 7.4) but are readily released from CaP-HDz-NP in endosomal/lysosomal pH conditions (pH 6 and 5). (d,e) Monitoring of enzyme-triggered NF degradation and drug release from NFs incorporated with both lipophilic drug, paclitaxel (PTX), and siRNA. To visualize NF degradation and drug release profile, the HDz-NPs were labled with Cy5.5 (HDz-Cy5.5), and PTX was labeled with Oregon green (PTX-OG). Fluorescent images of CaP-HDz-Cy5.5/PTX-OG/siRNA-NFs were collected after incubation with different concentrations (0, 2.5, 25, 250 units/mL) of Hyal in acetate buffer (pH = 4.3, 37 °C) for 1 h. When PTX-OG was compactly encapsulated in the NFs, the fluorescence of PTX-OG was highly quenched. However, after the NFs were incubated with Hyal, fluorescence intensities significantly increased, indicating NF degradation and consequent bursting release of PTX-OG from NFs.

analyses. The CaP-HDz/siRNA samples contained higher amount of siRNA compared with the free siRNA samples. After the serum incubation for 24 h, over 70% of siRNA loaded in the NFs were found to be intact, whereas free siRNA samples were completely degraded after 24 h incubation with serum. This indicates that CaP-HDz/siRNA-NFs can be maintained relatively stable in physiological serum conditions, protecting siRNAs from enzymatic degradation.

Prior to functional, biological studies, we examined the cellular uptake of HA/DPA-Zn-NP/siRNA in cancer cells (DU145 and 143B). To demonstrate cell permeation attributes of the NFs, we treated CD44-positive DU145 cancer cells with CaP-HDz/Cy3-RNA-NFs, Lipo2K/Cy3-RNA, or LipoMax/Cy3-RNA and monitored intracellular fluorescence signals using confocal fluorescence microscopy. We also confirmed the cellular uptake efficiency of CaP-HDz/Cy3-RNA in CD44-positive DU145 cancer cells. The transfection efficiency of Cy3-RNA was quantitatively evaluated using flow cytometry. Overall, the NFs readily penetrated into and were evenly distributed in cells 1 h after treatment. Strong fluorescence signals were detected in cells incubated with CaP-HDz/Cy3-RNA-NFs, whereas lower fluorescence signals were observed from cancer cells treated with Lipo2K/Cy3-RNA or LipoMax/Cy3-RNA. Mean fluorescence intensity of CaP-HDz/Cy3-RNA-NF group was 3.2- to 3.8-fold higher than that of Lipo2K/Cy3-RNA or LipoMax/Cy3-RNA group in both cell lines (Supporting Information Figure S5a−c).

To better understand if the HA receptor CD44 mediates endocytosis of the NFs, we performed competitive binding studies. CD44 receptors on 143B cells were first blocked with excess amount of free HA molecules, and then the cells were treated with Cy5.5-labeled CaP-HDz-NC complexed with Cy3-labeled RNA. After 1 h incubation, intracellular fluorescence signals were evaluated. The fluorescence intensities from both

Cy5.5-NCs and Cy3-RNAs considerably decreased compared to those from NF-treated HCT116 cells without CD44 blocking (Supporting Information Figure S5d). These results demonstrated that the strong interaction between the CD44 and HA shell of HDz-NCs plays a pivotal role in cell permeation, although the surface of the NFs is partially covered with a CaP layer. This shows that CaP-HDz/RNA-NFs can bind onto and permeate into cancer cells primarily *via* CD44-mediated endocytosis.

Furthermore, we studied endosomal escape traits of CaP-HDz/RNA-NFs. We labeled endosomes with endosome staining agent (LysoTracker Blue DND-22, Invitrogen) after 6 h incubation of cancer cells with CaP-HDz/Cy3-RNAs. RNAs and endosomes were then imaged using confocal fluorescence microscopy. After 6 h incubation, siRNAs were separated from NCs and endosomes. RNAs were evenly distributed in the cytoplasm, indicating that RNAs were successfully dissociated from NCs, escaped from the endosome, and distributed into the cytoplasm (Supporting Information Figure S6). The results may be due to the pH-dependent calcium and phosphate ion release in acidic pH environments of intracellular compartments like endosomes, which increases intraendosomal osmotic pressure and induces membrane disruption of endosomes and then escape of RNAs from endosomes.[26,27]

After intracellular trafficking of the NFs, we investigated RNAi-based gene silencing utility using CaP-HDz/RNAs-NFs. Since the aim of this research is to develop a versatile nanoplatform for *in vivo* RNA delivery, we prepared three types of NFs containing three different model RNAs: firefly luciferase (fLuc) gene-targeting siRNA (siLuc); green fluorescence protein (GFP) gene-targeting siRNA (siGFP); or microRNA-34a (miR34a). To evaluate the RNAi activity of the NFs *in vitro* and *in vivo*, we established three cancer cell lines that stably express fLuc, GFP, or miR34a reporter gene vector: 143B-fLuc, DU145-GFP, or HCT116-miR34a. The RNAi effect can thus be assessed by optical-imaging-based facile, quantitative evaluation methods. The ability of CaP-HDz-NCs to deliver aforementioned RNAs into the cancer cells was quantitatively evaluated by measuring expression levels of fLuc, GFP, or miR34a in 143B-fLuc, DU145-GFP, or HCT116-miR34a treated with CaP-HDz/siLuc, CaP-HDz/siGFP, or CaP-HDz/miR34a NFs, respectively. The cells treated with corresponding free RNAs or RNAs with Lipo2K or LipoMax were tested as negative or positive control groups. Free siLuc did not show any distinct fLuc gene suppression effect since cells do not readily take up large, negatively charged molecules. Negative control siRNA (siNC) formulated with NCs (CaP-HDz/siNC-NFs) or Lipo2K (Lipo2K/siNC) also did not display gene silencing effect. When formulated with CaP-HDz, only 71.2 $\pm$ 16.7 fmol of siLuc was needed to suppress the fLuc gene expression level by 50%. After the cells were treated with 5 pmol of siLuc incorporated with NFs, the fLuc gene expression level was dropped by 92.7 $\pm$ 2.5%. However, when siLuc is complexed with Lipo2K, almost 30 times higher dose of siLuc (1.9 $\pm$ 2.0 pmol) was needed to get 50% fLuc gene suppression (Figure 4a,b and Supporting Information Figure S7a,b).

The excellent gene silencing effect of CaP-HDz/siRNA-NFs was confirmed with a different siRNA (siGFP) in a DU145-GFP cancer cell line. As demonstrated with siLuc, treatment of free siGFP, CaP-HDz/siNC-NF, or Lipo2K/siNC did not achieve any gene knockdown in DU145-GFP cells (Figure 4f and Supporting Information Figure S7d,e). On the other hand, CaP-HDz/siGFP-NFs did suppress GFP gene expression by 50% at a siGFP dose of 60.7 $\pm$ 12.7 fmol after incubation with DU145-GFP cells for 24 h. Furthermore, at a siGFP dose of 0.3 pmol, the NFs reached 91.8 $\pm$ 0.5% gene silencing. A 17-fold higher dose of siGFP (5 pmol) complexed with Lipo2K only attained 77.6 $\pm$ 4.7% knockdown (Figure 4d,e). Many gene transfection systems are known to be cytotoxic due to their strong positive charges. This study also found that Lipo2K or LipoMax was associated with considerable cytotoxicity, showing relatively low cell viability in the range of 54.8 $\pm$ 3.5 to 56.5 $\pm$ 3.8% at 5 pmol RNA dose (Figure 4c). However, the CaP-HDz-NC system does not rely on positively charged materials to incorporate RNAs; the system is mainly composed of anionic biopolymer, hyaluronan. For this reason, CaP-HDz/RNAs-NFs showed little cytotoxicity toward 143B, DU145, or HCT116 cells (81.9 $\pm$ 4.7 to 103.02 $\pm$ 3.4% viability at 5 pmol RNA dose) despite their substantial RNAi efficacy (Figure 4c and Supporting Information Figure S7c). These results strongly support our hypothesis that this newly engineered, versatile RNA nanocarrier system could effectively deliver a variety of RNAs into cancer cells for RNAi applications. The NC system demonstrates superior RNA delivery efficiency to the conventional gene transfecting agents as well as significantly lower cytotoxicity than Lipo2K or LipoMax.

The utility of this RNA delivery system is primarily attributed to its tumor targetability and RNAi potency *in vivo*. To demonstrate *in vivo* applications of the NF, we investigated the biodistribution and tumor-targeting profile of the CaP-HDz/RNA-NFs labeled with Cy5.5 in a HCT116 xenograft mouse model. HCT116 tumor-bearing mice (n = 4) were intravenously injected with Cy5.5-labeled NFs (280 μL; RNA = 700 pmol), where siLuc was formulated with CaP-HDz-NCs as a model RNA. It can be noted that, from 3 h post-administration of Cy5.5-CaP-HDz/RNA-NFs, tumor was clearly delineated by strong fluorescence signals from the tumor tissue, which increased until 6 h before decreasing. Until 48 h post-injection, considerable fluorescence signal was still seen in the tumor sites (Figure 5a,b). *Ex vivo* images also exhibited strong fluorescence intensities in the tumor tissue. Noticeable fluorescence

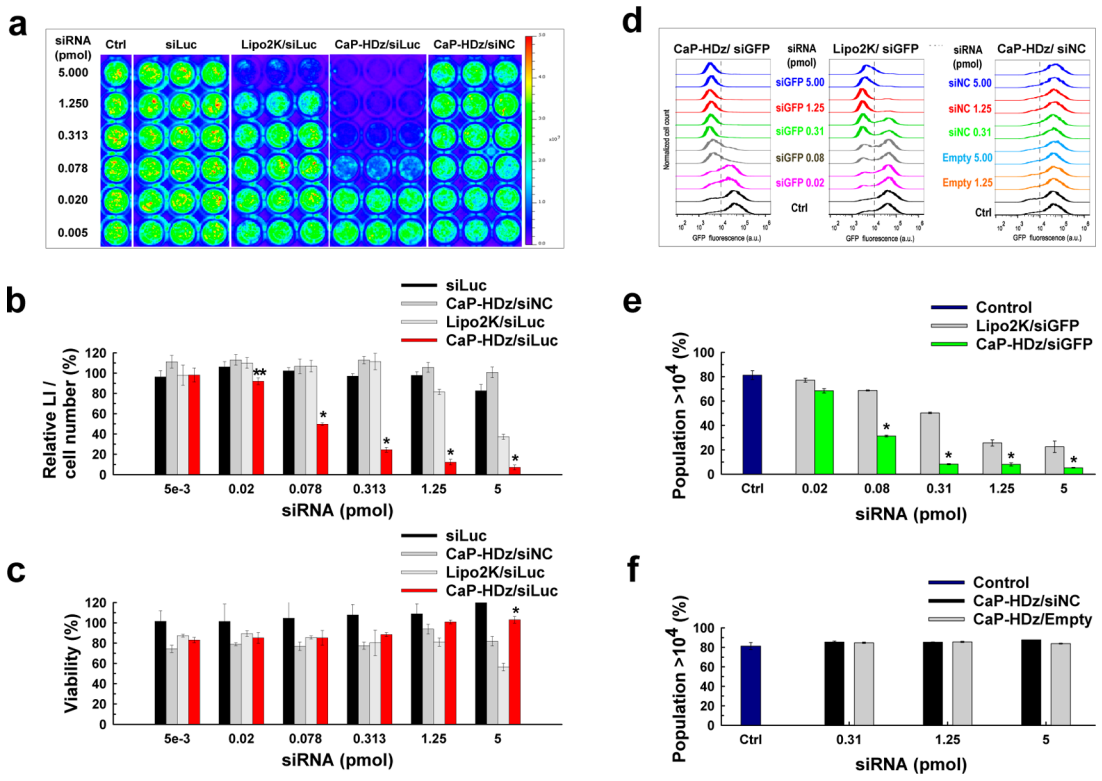

Figure 4. Suppression of gene expression using CaP-HDz/siRNA-NF. Suppression of fLuc gene expression and viability of 143B-fLuc cells after treatment with siRNA (siLuc or siNC) only, CaP-HDz-NP or Lipo2K complexed with siLuc or siNC (a,b and Supporting Information Figure S5a,b); *$p < 0.005$, **$p < 0.05$ *vs* control or Lipo2K/siLuc. CaP-HDz/siLuc group suppresses fLuc genes more efficiently than the Lipo2K/siLuc or free siLuc group. The CaP-HDz-NP group also shows less toxicity compared to the Lipo2K group at high concentrations (c and Supporting Information Figure S5c). Suppression effect of CaP-HDz/siRNA-NFs was confirmed with siGFP in DU145-GFP cells. Suppression of GFP gene expression of DU145-GFP cells by CaP-HDz-NP or Lipo2K complexed with siGFP, siNC, or empty carriers (CaP-HDZ-NP or Lipo2K) without RNA complexation (d–f and Supporting Information Figure S5d,e); *$p < 0.005$ *vs* control group or Lipo2K/siGFP group. The CaP-HDz/siGFP group shows suppresion of the GFP gene expression more efficiently than the Lipo2K/siGFP group. However, the siNC or empty groups do not show notable suppression effect.

signal was also found in the liver and kidneys (Supporting Information Figure S8a,b).

Furthermore, we studied the tumor-specific RNAi effect of CaP-HDz/RNA-NFs in a HCT116 xenograft model. We intravenously administered PBS, CaP-HDz/siLuc-NFs, or CaP-HDz/siNC-NFs (280 μL; RNA = 700 pmol) into the tumor-bearing mice. The fLuc gene silencing efficiency was quantitatively estimated by *in vivo* BLI. At 72 h post-injection, the BL intensities from tumors of the CaP-HDz/siLuc-NF group dramatically lessened, indicating significant suppression of fLuc gene expression but not from tumors of the other groups (PBS, CaP-HDz/siNC-NF). The fLuc gene expression in the tumors of CaP-HDz/siLuc-NF groups was inhibited by 79.4 $\pm$ 11.7%, such that the bioluminescence signal was barely observed in the tumors (Figure 5c,d). On the other hand, the BL signals in the tumors of PBS and CaP-HDz/siNC-NF groups were greatly amplified. The fLuc gene expression was augmented by 49.7 $\pm$ 3.3 and 32.3 $\pm$ 15.8% in the PBS and CaP-HDz/siNC-NF groups, respectively, which can account presumably dye to tumor cell proliferation.

The remarkable ability of CaP-HDz-NCs to deliver RNAs is not confined to siRNA delivery but can also be applied to miRNA-based RNAi. To assess miR34a transfection efficiency of CaP-HDz/miR34a-NFs, we established a stable cell line transfected with a miR34a imaging reporter system that generates a strong cellular bioluminescence signal. Presence of intracellular miR34a decreases the BL signals in a dose-dependent manner. We quantitatively examined the intracellular level of miR34a transfected by CaP-HDz-NCs or the second-generation RNA transfection agent, LipoMax (RNAiMAX), by measuring BL intensity in HCT116-miR34a cells treated with CaP-HDz/miR34a-NFs or LipoMax/miR34a. The CaP-HDz-NC system effectively delivered miR34a molecules into the cytoplasm. CaP-HDz/miR34a could reach a 50% signal decrease with a miR34a dose of 0.1 $\pm$ 0.003 pmol, whereas LipoMax requires almost 10 times higher miRNA dose of 1.2 $\pm$ 0.2 pmol to reach the same effect (Figure 6a–d).

We also assessed the *in vivo* miRNA delivery activity using CaP-HDz/miR34a-NF. CaP-HDz/miR34a-NFs were systemically injected into mice bearing HCT116-miR34a tumors. PBS or CaP-HDz/miRNC-NFs were also administered as controls (280 μL; RNA = 700 pmol). After 24 h, BL intensities at tumors of CaP-HDz/miR34a-NF group

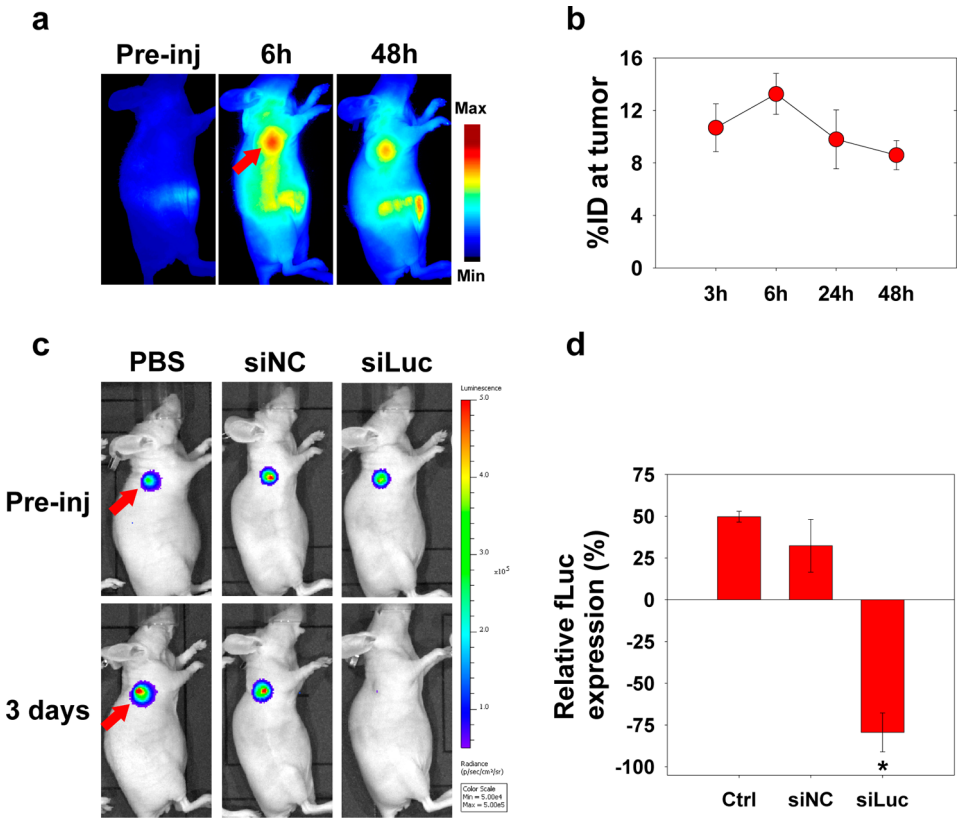

Figure 5. ***In vivo*** **monitoring of tumor-targeting and gene silencing effect of CaP-HDz/siRNA-NFs. (a)** ***In vivo*** **near-infrared fluorescence (NIRF) imaging of HCT116 tumor-bearing mice systemically administered with CaP-HDz/siLuc-NFs labeled with Cy5.5. (b) Quantitative analysis of fluorescence intensities at the tumor site of mice treated with CaP-HDz/siLuc-NFs. The % ID indicates the percentage of the injected dose. Error bars represent SD (*n* = 4). NIRF signals for the NFs at the tumor site were strong enough to outline tumors. The NIRF imaging revealed that the NFs accumulated at the tumor site until 6 h and were then slowly cleared from tumors. (c)** ***In vivo*** **bioluminescence imaging (BLI) of fLuc gene expression in fLuc-expressing HCT116 tumor-bearing mice intravenously injected with PBS, free siLuc, or CaP-HDz/siLuc-NFs (280 μL; RNA = 700 pmol). (d) Quantitative analysis of fLuc expression at tumors after intravenous injection of CaP-HDz/siLuc-NFs into the fLuc-expressing HCT116 tumor mice (*n* = 4). The BL intensities from tumors of the CaP-HDz/siLuc-NF group significantly decreased at 3 days after injection, implying effective suppression of fLuc gene expression but not from tumors of the other groups (PBS, CaP-HDz/siNC-NF). Red arrow indicates tumor site; **p* < 0.005, ***p* < 0.05** ***vs*** **control or siNC.**

substantially dropped by 52.9 ± 19.5%, indicating effective intracellular delivery of miR34a into tumor cells by the NFs *in vivo* (Figure 6e,f). However, the BL intensities from the control groups markedly increased by 33.3 ± 10.2% (PBS) or 39.9 ± 7.9% (CaP-HDz/siNC-NF). While measuring BL intensities, we did not find noticeable decrease in tumor size of all the groups, implying that the decrease in BL signal was induced by successful intracellular delivery of miRNA rather than the cytotoxicity of the nanoformula.

Recently, we have also established advanced NFs coloaded with chemo- and RNAi therapeutics for synergistic tumor therapy. As a proof-of-concept study, the drug/RNA codelivery was monitored in HCT116 cancer cells (Supporting Information Figure S9). Both a model drug, paclitaxel labeled with Oregon green (OG-PTX), and Cy3-labeled siRNA could be delivered in HCT116 cancer cells within 30 min after treatment, showing rapid internalization of CaP-HDz/drug/RNA-NFs. Furthermore, to validate therapeutic utility of CaP-HDz/drug/RNA-NFs, we also formulated an anticancer drug, doxorubicin (Dox), along with siMDR in CaP-HDz nanoparticles (CaP-HDz/Dox/siMDR-NFs).

In an effort to substantiate therapeutic potential of the NFs, we investigated the RNAi effects of the CaP-HDz/RNA-NFs on a therapeutic target protein, p-glycoprotein 1 (P-gp1) expression (also referred to as multidrug resistance protein 1 (MDR1)), which is known to be ascribed to multidrug resistance traits of various cancer cells.[30] We complexed MDR1-target siRNA (siMDR) with CaP-HDz nanocarriers. After drug-resistant OVCAR8 (OVCAR8/ADR) cells were treated with CaP-HDz/siMDR-NFs, the MDR1 mRNA and P-gp1 expression levels were examined by qRT-PCT and Western blot analyses. CaP-HDz/siMDR-NFs significantly down regulated both MDR1 mRNA and P-gp1 expression (Supporting Information Figure S10), which indicates the recovery of sensitivity of OVCAR8/ADR cells to drugs.

Furthermore, therapeutic activity of NFs coloaded with Dox and siMDR (CaP-HDz/Dox/siMDR-NFs) was evaluated *in vitro* by monitoring the viability of

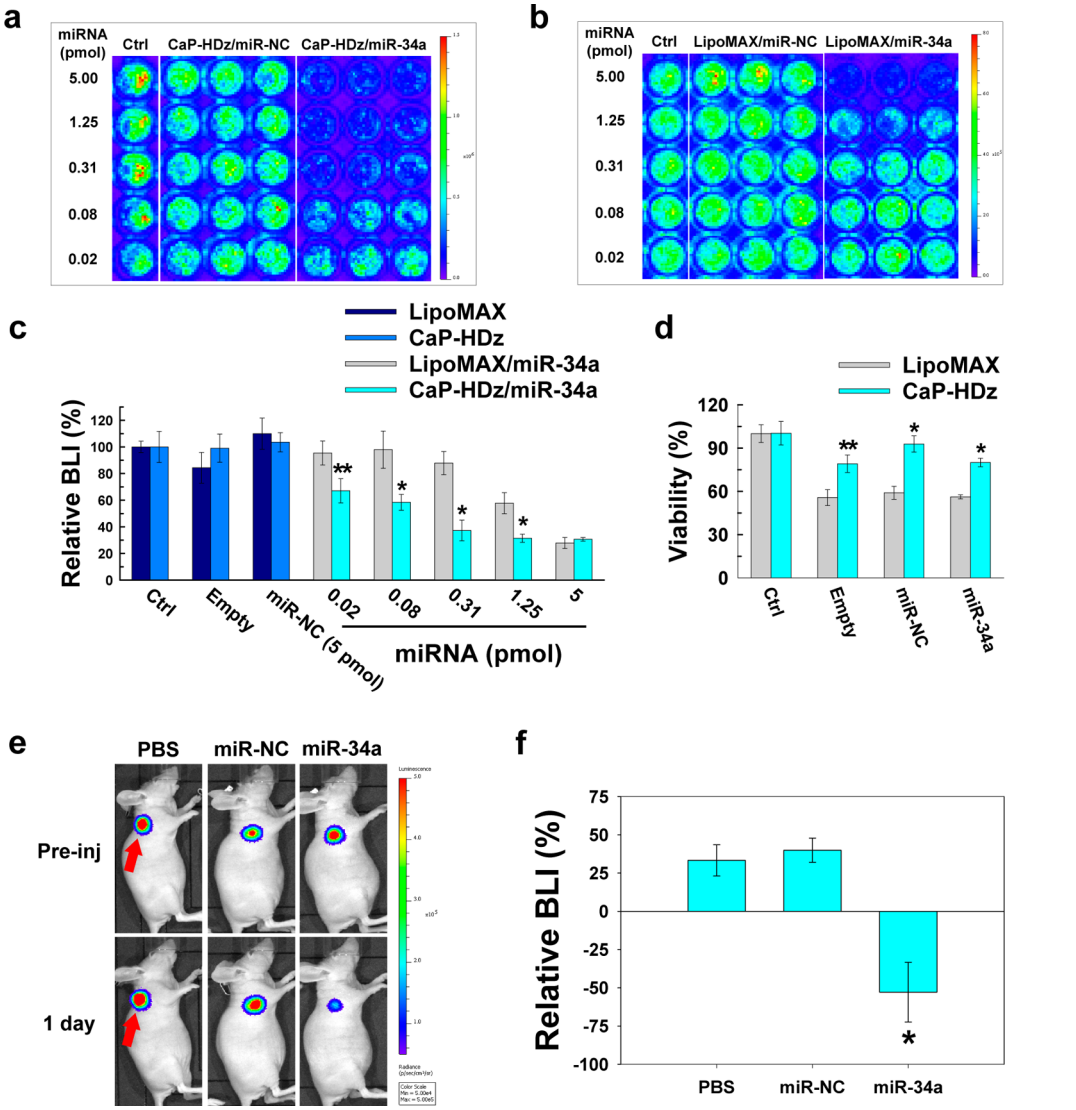

Figure 6. Tumor-cell-specific miR34a delivery using CaP-HDz/miR34a-NFs. Delivery of miRNA into HCT116-fLuc-miR34a cells by CaP-HDz-NP (a) or LipoMAX (b) complexed with miR34a, miR-NC, or empty carriers without complexation. (c) Quantitative analysis of miR34a delivery efficiency using a BLI technique. HCT116-fLuc-miR34a cells are designed to express strong BL signals. Once miR34a is delivered into the HCT116 cells, it can bind with miR34a binding domain in the cells and rapidly suppress BL signals, and thus the BL intensity can be used for quantification of intracellular concentration of miR34a. (d) Viability of HCT116 cells after treatment of CaP-HDz or LipoMAX complexed with miRNA (5 pmol) or empty carriers; *$p < 0.005$, **$p < 0.05$ *vs* the control or LipoMAX/miRNA groups. CaP-HDz/miR34a group suppresses fLuc signals more efficiently than the LipoMAX/miR34a group. The CaP-HDz-NP group also shows less toxicity compared to the LipoMAX group at the high concentration (5 pmol). (e) *In vivo* bioluminescence imaging of HCT116-fLuc-miR34a tumor-bearing mice intravenously injected with PBS, free miR34a, or CaP-HDz/miR34a-NFs (280 μL; RNA = 700 pmol). (f) Quantitative analysis of miR34a delivery efficiency at tumors after intravenous injection of CaP-HDz/miR34a-NFs into the HCT116-fLuc-miR34a xenograft ($n = 4$). The BL signals from tumors of the CaP-HDz/siLuc-NF group significantly decreased *in vivo* as well as *in vitro*, suggesting effective miR34a delivery, but not from tumors of the other groups (PBS, CaP-HDz/siNC-NF); *$p < 0.005$ *vs* control or miRNC.

OVCAR8/ADR cells after treatment with free Dox, CaP-HDz/Dox/siNC, or CaP-HDz/Dox/siMDR-NFs as well as *in vivo* by measuring tumor volume of OVCAR8/ADR xenografted mice after systemic administration of saline, free Dox, CaP-HDz/Dox/siNC, or CaP-HDz/Dox/siMDR-NFs. Treatment of CaP-HDz/Dox/siMDR-NFs exhibited significantly superior suppression effects not only on the OVCAR8/ADR tumor cell proliferation (Figure 7a) *in vitro* but also on the growth of OVCAR8/ADR tumor *in vivo* (Figure 7b) as compared to that of free Dox, CaP-HDz/Dox, or CaP-HDz/Dox/siNC.

CONCLUSIONS

Development of nontoxic, tumor-targetable, and potent *in vivo* RNAi delivery systems remains a formidable challenge. In this study, we developed a versatile RNAi nanoplatform based on a tumor-targeting and pH-responsive RNA nanoformula. The NF was engineered by combination of tumor-targeted HA nanoparticle with an artificial RNA receptor, Zn(II)-DPA, which was further protected with a CaP coating by *in situ* mineralization. The NF can strongly secure RNA molecules through the

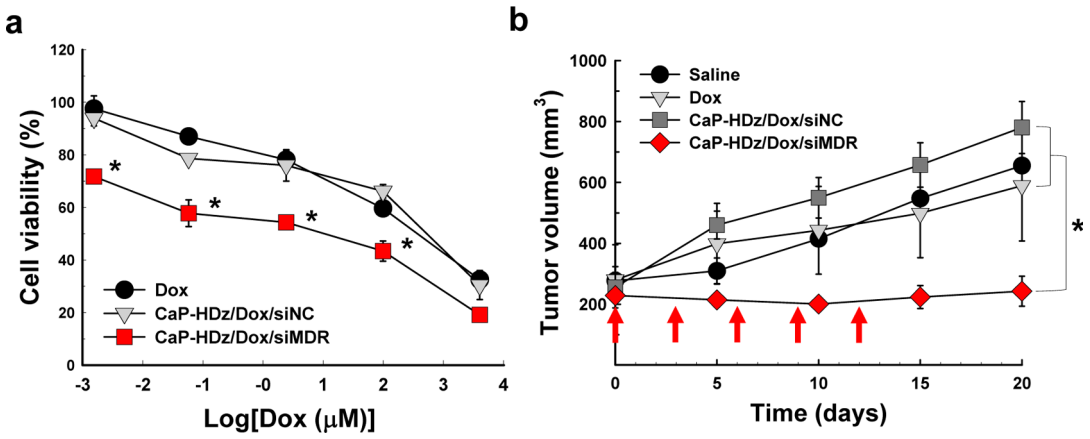

Figure 7. Therapeutic activity of CaP-HDz/Dox/siMDR-NFs against Dox-resistant OVCAR8 cells. Antitumor efficacy of CaP-HDz/Dox/siMDR-NFs in drug-resistant OVCAR8/ADR cells (n = 6) (a) or in OVCAR8/ADR tumor-bearing mice (n = 4) (b) after systemic administration of the NFs. OVCAR8/ADR tumor cells were remarkably sensitized to Dox when siMDR is formulated with Dox in CaP-HD nanocarriers, showing significantly improved therapeutic activity compared to the free Dox or CaP-HDz/Dox/siNC; *p < 0.005 *vs* free Dox or CaP-HDz/Dox/siNC.

artificial RNA receptors as well as the robust CaP coating and also can target RNAs into the tumor cells *in vivo* through both passive targeting and CD44-mediated endocytosis. The NF can eventually distribute RNAs into the cytosol of cancer cells, selectively suppressing target gene expression. Unlike most reported gene delivery systems, this NF system is not based on cationic derivatives to incorporate nucleic acid derivatives, and thus the NF demonstrated much lower nonspecific accumulation and toxicity yet higher tumor targetability and tumor-specific gene delivery efficacy after systemic administration than the conventional gene transfection agents. This NF system can be used as a versatile delivery platform for RNAi and nanomedicine application, which may open up new possibilities for RNA-based cancer therapeutics.

METHODS

Chemical structures, synthesis schemes, and detailed experimental methods are described in the Supporting Information. All animal experiments were conducted in accordance with an NIH approved protocol.

Materials. Sodium hyanluronate (M_w 200 K) was purchased from Lifecore Biomedical (Chaska, MN, USA). Cells were purchased from the American Type Culture Collection (Rockville, MD, USA). The other chemicals and biological materials were purchased from Sigma-Aldrich Co. (St. Louis, MO, USA) or Invitrogen (Carlsbad, CA, USA) unless otherwise noted.

Synthesis of HDz Nanoparticle. HA-based nanoparticles conjugated with an artificial RNA receptor, DPA/Zn, were synthesized. First, we synthesized amine-functionalized bis(DPA) molecules and amphiphilic HA-CA conjugates. To prepare HA-based nanoparticles (HA-NPs), HA-CA conjugates (60 mg) were dispersed in 12 mL of DW using a probe-type sonifier for 20 min. Second, bis(DPA) molecules (15 mg, 27 μmol), as an RNA receptor, were chemically conjugated onto HA-NPs through amide formation in the presence of EDC (10.5 mg, 54 μmol) and sulfu-NHS (17.6 mg, 81 μmol). The HA-NPs modified with DPA molecules (HD-NPs) were purified by dialysis against distilled water for 24 h and were freeze-dried to get a dried white powder. Third, to complex Zn ions with DPA ligands (HDz-NPs), zinc nitrate hexahydrate (ZNH) (5 mL, 3 mg/mL, 10.1 mM) was mixed with HD-NPs (5 mL, 2 mg/mL in UPW), and the resulting mixture was incubated at 40 °C under agitation for 30 min. The structure and purity of the HDz conjugate were analyzed by ^{1}H NMR and RP-HPLC, respectively.

Formulation of Chemotherapeutics. HDz-NPs can be loaded with biological therapeutics (RNAs) and chemotherapeutics (small-molecule hydrophobic drugs). Small-molecule chemotherapeutics can be encapsulated within the hydrophobic within HDz-NPs by strong interaction between hydrophobic CA molecules of NPs and hydrophobic drug molecules using a sonication method in aqueous solution. To prepare drug/RNA coloaded NFs, drug encapsulation should be preceded by RNA formulation. First, we dispersed HDz conjugate in UPW at 5 mg/mL by sonication using a probe-type sonifier for 20 min. Small-molecule drug molecules (paclitaxel labeled with Oregon green (PTX-OG) or doxorubicin (Dox)) dissolved in DMF (4 mg/mL) were added dropwise into the HDz-NP solution (2 mL) during sonication for 20 min. The solution was agitated for 30 min with stirring and dialyzed against distilled water for 12 h using dialysis tubing (12−14 K MWCO) to remove DMF and unloaded residues, followed by the freeze-dry. Drug contents in the NFs were calculated by RP-HPLC after the nanoformulas were disassembled in DW/DMF (1/1 v/v) cosolvent.

Formulation of RNA Therapeutics. To prepare HDz-NPs, we dispersed HDz conjugate (or HDz/PTX-NPs) in UPW at 1 mg/mL by sonication using a probe-type sonifier for 20 min. The HDz-NP solution (2 μL) was vigorously mixed with 1 μL of RNAs, that is, firefly luciferase target siRNA (siLuc), microRNA-34a (miR34a), or oligonucleotide 623 (Oligo-623), and the solution was incubated at room temperature for 30 min. Moreover, we deposited inorganic calcium phosphate (CaP) layers onto the nanoformulas by *in situ* mineralization method to provide further protection of RNA molecules. We added 1 μL of Tris-calcium buffer (1 mM Tris, 250 m $CaCl_2$, pH 7.6) and sequentially added 4 μL of HEPES phosphate buffer (50 mM HEPES, 1.5 mM Na_2HPO_4, pH 7.4) onto the HDz/siRNA nanoformulas. The solution was vigorously agitated by pipetting. The CaP-doped HDz/RNA (CaP-HDz/RNA or CaP-HDz/PTX/RNA) nanoformulas were treated for *in vitro*/*in vivo* application after incubated for 5 min at room temperature.

Gene Silencing Effects of CaP-HDz/RNAs in Cells. We established stabilized cell lines: 143B cells, DU145, and HCT116 cells expressing firefly luciferase gene (fLuc), green fluorescence protein, or miR34a reporter gene vector (143B-fLuc, DU145-GFP, HCT116-fLuc, or HCT116-miR34a). 143B, DU145, and HCT116 cells were

maintained in MEM medium with 10% FBS at 37 °C in a humidified 5% CO_2 atmosphere. Cells were transfected with pcDNA3.1 expression vector modified with fLuc, GFP, or with the inclusion of one miR34a perfect binding site (ACAACCAGCTAAGACACTGCCA) in the 3′ UTR of fLuc protein using Lipo2K based on the protocol for Lipo2K provided by the company (Invitrogen). We added the selection reagent Geneticin (G418) onto the cells transfected with fLuc, GFP, or miR34a vector, and colonies showing significant signals were selected after monitoring fLuc or GFP expression level. To confirm gene silencing effects of CaP-HDz/RNA nanoformulas, we seeded cells in 96-well plates and treated the cells with CaP-HDz/siLuc, CaP-HDz/GFP, or CaP-HDz/miR34a (8 μL; siRNA = 10 pmol) dispersed in 92 μL of the cell culture medium (MEM, 10% FBS). Cells were incubated for 24 h. Parallel experiments for positive control (Lipo2K/siLuc, Lipo2K/GFP, or LipoMAX/miR34a) and negative control (CaP-HDz/siNC or CaP-HDz/miNC) were also carried out. After 24 h incubation, the fLuc or GFP signals in the cells were quantified using a flow cytometer (BD Accuri C6) or a bioluminnescence imaging system (Xenogen IVIS-100), respectively. The bioluminescence or fluorescence intensity (BLI or FI) of untreated cells is set as the 100% signal intensity, and the relative BLI or FI is calculated to estimate the fLuc, GFP gene expression level, or intracellular miR34a level. The BLI signal intensity is further normalized with live cell numbers. The cytotoxicity of HDz/RNAs, CaP-HDz/RNAs, or Lipo/RNAs was assessed according to the alamarBlue assay protocol.

***In Vivo* Gene Silencing Effects of CaP-HDz/RNAs.** HCT116 tumor xenograft models were prepared by subcutaneous injection of 5×10^6 HCT116-miR34a cells in the right flank of female athymic nude mice (18−20 g). When the diameter of tumors reached about 8 mm, CaP-HDz/siLuc or CaP-HDz/miR34a (280 μL; RNA = 700 pmol) was intravenously administrated into the mice. In parallel, CaP-HDz/siNC, CaP-HDz/miNC (280 μL; RNA = 700 pmol), or 280 μL of PBS was also injected as control groups. The BLI was visualized by Xenogen IVIS-100, and the relative fLuc expression level was calculated as previously reported.[24]

***In Vitro* Cytotoxicity of CaP-HDz/Dox/siMDR-NFs.** The cytotoxic effects of Dox, CaP-HDz/Dox/siNC, and CaP-HDz/Dox/siMDR were evaluated using the alamarBlue assay (Life Technologies). OVCAR8/ADR cells were seeded at a density of 1×10^4 cells/well in 96-well flat-bottomed plates and incubated for 48 h. Cells were washed twice with PBS and incubated in the culture medium with various concentrations of Dox, CaP-HDz/Dox/siNC, and CaP-HDz/Dox/siMDR for 48 h at 37 °C. Cell viability was evaluated according to the alamarBlue assay protocol.

***In Vivo* Antitumor Efficacy of CaP-HDz/Dox/siMDR-NFs.** To evaluate the antitumor efficacy of CaP-HDz/Dox/siMDR, OVCAR8/ADR tumor-bearing mice were prepared: A suspension of 1×10^7 OVCAR8/ADR ovarian cancer cells was subcutaneously injected into the right flank of 5−6 week old female athymic nude mice (18−20 g). When tumors reached ∼8 mm in diameter, each treatment was injected five times every 3 days. Four treatment groups: (i) saline (280 μL, the control group), (ii) free Dox (280 μL; 50 μg), (iii) CaP-HDz/Dox/siNC-NFs (280 μL; Dox = 50 μg; siNC 700 pmol), and (iv) CaP-HDz/Dox/siMDR-NFs (280 μL; Dox = 50 μg; siMDR 700 pmol). Tumor volumes were calculated as $a \times b^2/2$, where a is the largest and b is the smallest diameter.

Statistical Analysis. The statistical significance of differences among the groups tested was determined with Sigma Plot using t-test. A p value less than 0.05 is considered significant and is specified in the figures with an asterisk: $^*p < 0.005$, $^{**}p < 0.05$.

Conflict of Interest: The authors declare no competing financial interest.

Acknowledgment. This work was supported by the Intramural Research Program of the National Institute of Biomedical Imaging and Bioengineering (NIBIB), National Institutes of Health (NIH), and partially supported by an AXA Research Fund Postdoctoral Fellowship, the NRF Postdoctoral Fellowship (2013R1A6A3A03) and NRF grant (2009-0080734) funded by the Korea government (MSIP). The authors thank the input of Ms. Myung Sun Lee for illustrations.

Supporting Information Available: Synthesis schemes (Figure S1). Chemical structure and NMR spectrum (Figure S2). RNA sequences (Table S1). AFM analyses (Figure S3). Cellular uptake and RNA transfection (Figure S4). Cellular imaging of endosomal escape (Figure S5). RNA stability analysis (Figure S6). Suppression of gene expression (Figure S7). *Ex vivo* tissue distribution (Figure S8). Intracellular delivery of drug and RNA (Figure S10). qRT-PCR and Western blot analyses (Figure S9). Supporting Information methods are also described in the Supporting Information. This material is available free of charge *via* the Internet at http://pubs.acs.org.

REFERENCES AND NOTES

1. Elbashir, S. M.; Harborth, J.; Lendeckel, W.; Yalcin, A.; Weber, K.; Tuschl, T. Duplexes of 21-Nucleotide RNAs Mediate RNA Interference in Cultured Mammalian Cells. *Nature* **2001**, *411*, 494–498.
2. de Fougerolles, A.; Vornlocher, H. P.; Maraganore, J.; Lieberman, J. Interfering with Disease: A Progress Report on siRNA-Based Therapeutics. *Nat. Rev. Drug Discovery* **2007**, *6*, 443–453.
3. Kong, Y. W.; Ferland-McCollough, D.; Jackson, T. J.; Bushell, M. MicroRNAs in Cancer Management. *Lancet Oncol.* **2012**, *13*, e249–258.
4. Kumar, P.; Ban, H. S.; Kim, S. S.; Wu, H.; Pearson, T.; Greiner, D. L.; Laouar, A.; Yao, J.; Haridas, V.; Habiro, K.; *et al.* T Cell-Specific siRNA Delivery Suppresses HIV-1 Infection in Humanized Mice. *Cell* **2008**, *134*, 577–586.
5. Eguchi, A.; Meade, B. R.; Chang, Y. C.; Fredrickson, C. T.; Willert, K.; Puri, N.; Dowdy, S. F. Efficient siRNA Delivery into Primary Cells by a Peptide Transduction Domain-dsRNA Binding Domain Fusion Protein. *Nat. Biotechnol.* **2009**, *27*, 567–571.
6. Endoh, T.; Ohtsuki, T. Cellular siRNA Delivery Using Cell-Penetrating Peptides Modified for Endosomal Escape. *Adv. Drug Delivery Rev.* **2009**, *61*, 704–709.
7. Lee, J. B.; Hong, J.; Bonner, D. K.; Poon, Z.; Hammond, P. T. Self-Assembled RNA Interference Microsponges for Efficient siRNA Delivery. *Nat. Mater.* **2012**, *11*, 316–322.
8. Mok, H.; Lee, S. H.; Park, J. W.; Park, T. G. Multimeric Small Interfering Ribonucleic Acid for Highly Efficient Sequence-Specific Gene Silencing. *Nat. Mater.* **2010**, *9*, 272–278.
9. Tseng, Y. C.; Mozumdar, S.; Huang, L. Lipid-Based Systemic Delivery of siRNA. *Adv. Drug Delivery Rev.* **2009**, *61*, 721–731.
10. Akinc, A.; Zumbuehl, A.; Goldberg, M.; Leshchiner, E. S.; Busini, V.; Hossain, N.; Bacallado, S. A.; Nguyen, D. N.; Fuller, J.; Alvarez, R.; *et al.* A Combinatorial Library of Lipid-like Materials for Delivery of RNAi Therapeutics. *Nat. Biotechnol.* **2008**, *26*, 561–569.
11. Whitehead, K. A.; Langer, R.; Anderson, D. G. Knocking Down Barriers: Advances in siRNA Delivery. *Nat. Rev. Drug Discovery* **2009**, *8*, 129–138.
12. Oh, Y. K.; Park, T. G. siRNA Delivery Systems for Cancer Treatment. *Adv. Drug Delivery Rev.* **2009**, *61*, 850–862.
13. Daka, A.; Peer, D. RNAi-Based Nanomedicines for Targeted Personalized Therapy. *Adv. Drug Delivery Rev.* **2012**, *64*, 1508–1521.
14. Choi, K. Y.; Chung, H.; Min, K. H.; Yoon, H. Y.; Kim, K.; Park, J. H.; Kwon, I. C.; Jeong, S. Y. Self-Assembled Hyaluronic Acid Nanoparticles for Active Tumor Targeting. *Biomaterials* **2010**, *31*, 106–114.
15. Choi, K. Y.; Min, K. H.; Na, J. H.; Choi, K.; Kim, K.; Park, J. H.; Kwon, I. C.; Jeong, S. Y. Self-Assembled Hyaluronic Acid Nanoparticles as a Potential Drug Carrier for Cancer Therapy: Synthesis, Characterization, and *In Vivo* Biodistribution. *J. Mater. Chem.* **2009**, *19*, 4102–4107.
16. Choi, K. Y.; Jeon, E. J.; Yoon, H. Y.; Lee, B. S.; Na, J. H.; Min, K. H.; Kim, S. Y.; Myung, S. J.; Lee, S.; Chen, X.; *et al.* Theranostic Nanoparticles Based on PEGylated Hyaluronic Acid for the Diagnosis, Therapy and Monitoring of Colon Cancer. *Biomaterials* **2012**, *33*, 6186–6193.
17. Choi, K. Y.; Yoon, H. Y.; Kim, J. H.; Bae, S. M.; Park, R. W.; Kang, Y. M.; Kim, I. S.; Kwon, I. C.; Choi, K.; Jeong, S. Y.; *et al.* Smart Nanocarrier Based on PEGylated Hyaluronic Acid for Cancer Therapy. *ACS Nano* **2011**, *5*, 8591–8599.

18. Toole, B. P.; Slomiany, M. G. Hyaluronan: A Constitutive Regulator of Chemoresistance and Malignancy in Cancer Cells. *Semin. Cancer Biol.* **2008**, *18*, 244–250.
19. Toole, B. P. Hyaluronan: From Extracellular Glue to Pericellular Cue. *Nat. Rev. Cancer* **2004**, *4*, 528–539.
20. Choi, K. Y.; Saravanakumar, G.; Park, J. H.; Park, K. Hyaluronic Acid-Based Nanocarriers for Intracellular Targeting: Interfacial Interactions with Proteins in Cancer. *Colloids Surf., B* **2012**, *99*, 82–94.
21. Rhee, H. W.; Choi, S. J.; Yoo, S. H.; Jang, Y. O.; Park, H. H.; Pinto, R. M.; Cameselle, J. C.; Sandoval, F. J.; Roje, S.; Han, K.; *et al.* A Bifunctional Molecule as an Artificial Flavin Mononucleotide Cyclase and a Chemosensor for Selective Fluorescent Detection of Flavins. *J. Am. Chem. Soc.* **2009**, *131*, 10107–10112.
22. Wyffels, L.; Gray, B. D.; Barber, C.; Moore, S. K.; Woolfenden, J. M.; Pak, K. Y.; Liu, Z. Synthesis and Preliminary Evaluation of Radiolabeled Bis(zinc(II)-dipicolylamine) Coordination Complexes as Cell Death Imaging Agents. *Bioorg. Med. Chem.* **2011**, *19*, 3425–3433.
23. Rhee, H. W.; Lee, S. H.; Shin, I. S.; Choi, S. J.; Park, H. H.; Han, K.; Park, T. H.; Hong, J. I. Detection of Kinase Activity Using Versatile Fluorescence Quencher Probes. *Angew. Chem., Int. Ed.* **2010**, *49*, 4919–4923.
24. Liu, G.; Choi, K. Y.; Bhirde, A.; Swierczewska, M.; Yin, J.; Lee, S. W.; Park, J. H.; Hong, J. I.; Xie, J.; Niu, G.; *et al.* Sticky Nanoparticles: A Platform for siRNA Delivery by a Bis(zinc(II) dipicolylamine)-Functionalized, Self-Assembled Nanoconjugate. *Angew. Chem., Int. Ed.* **2012**, *51*, 445–449.
25. Rim, H. P.; Min, K. H.; Lee, H. J.; Jeong, S. Y.; Lee, S. C. pH-Tunable Calcium Phosphate Covered Mesoporous Silica Nanocontainers for Intracellular Controlled Release of Guest Drugs. *Angew. Chem., Int. Ed.* **2011**, *50*, 8853–8857.
26. Li, J.; Chen, Y. C.; Tseng, Y. C.; Mozumdar, S.; Huang, L. Biodegradable Calcium Phosphate Nanoparticle with Lipid Coating for Systemic siRNA Delivery. *J. Controlled Release* **2010**, *142*, 416–421.
27. Guo, S.; Huang, L. Nanoparticles Escaping RES and Endosome: Challenges for siRNA Delivery for Cancer Therapy. *J. Nanomater.* **2011**, *2011*, 1–12.
28. Stern, R.; Jedrzejas, M. J. Hyaluronidases: Their Genomics, Structures, and Mechanisms of Action. *Chem. Rev.* **2006**, *106*, 818–839.
29. Stern, R. Hyaluronidases in Cancer Biology. *Semin. Cancer Biol.* **2008**, *18*, 275–280.
30. Gottesman, M. M.; Fojo, T.; Bates, S. E. Multidrug Resistance in Cancer: Role of ATP-Dependent Transporters. *Nat. Rev. Cancer* **2002**, *2*, 48–58.